Composites Science and Technology 192 (2020) 108115

Contents lists available at ScienceDirect

Composites Science and Technology

journal homepage: http://www.elsevier.com/locate/compscitech

Magnetically tunable adhesion of composite pads with magnetorheological polymer gel cores

Haoming Pang [a,b], Lei Pei [a], Jiaqi Xu [a], Saisai Cao [a], Yu Wang [a,**], Xinglong Gong [a,*]

[a] CAS Key Laboratory of Mechanical Behavior and Design of Materials, Department of Modern Mechanics, CAS Center for Excellence in Complex System Mechanics, University of Science and Technology of China (USTC), Hefei, 230027, PR China
[b] Postdoctoral Research Center, Anhui Weiwei Rubber Parts Group Co. Ltd, Tongcheng, 231400, PR China

ARTICLE INFO

Keywords:
Adhesion
Magnetic field
Composite structure
Interface stress
Core shapes

ABSTRACT

Tunable and reversible dry adhesion has important applications in transfer printing, precision manufacturing, and intelligent robotics. In this paper, a novel composite pad is fabricated whose adhesion can be adjusted rapidly and reversibly by the magnetic field. The composite pad consists of a cylindrical polydimethylsiloxane (PDMS) shell and a magnetorheological polymer gel (MRPG) core. The mechanical properties of the MRPG core in the pads are sensitive to the magnetic field. So the adhesion of the composite pad can be changed due to the interface stress modulation by the magnetic field. The interface stress is calculated by using the finite element method to study the mechanism of magnetically controllable adhesion. The results show the smaller the edge stress, the larger the adhesion. So composite pads with four different core shapes are prepared to optimize the structure design. Pad-bump has the largest magnetically tunable adhesion interval. The adhesion of composite pads on uneven surfaces is also tested and the results show the adhesion of composite pads with soft cores is improved compared to the solid core pad. Finally, a magnetic field controlled pick-and-place demonstration experiment shows that the composite pad array has great application potential in magnetically controlled grabbing and release.

1. Introduction

Tunable and reversible dry adhesion is common in nature. Geckos and insects can achieve repeated cycles of attachment and detachment using hairy structures on footpads. In modern industry, repeatable adhesion plays an important role in controlling grip, movement, etc., and thus has many applications in the field of transfer printing [1–5], precision manufacturing [6,7], and intelligent robotics [8,9].

Inspired by nature, various structures with reversible adhesion have been thoroughly investigated over the last decade. The surface morphology of these insect feet has a common feature, that is, the surface has dense elongated fibrillar structures. Bullock and Federle studied the effect of fibril shape on adhesion and found that mushroom-shaped tips had the largest pull off force [10]. However, the adhesion of these structures does not change once they are prepared. The gecko-inspired surface provides an effective path to tunable dry adhesive [11–13]. The switching in adhesion is achieved by using fibrillar structures with angled or asymmetric geometries [14–17], a reversible buckling of adhesive pillar structures [18,19], and changing the loading modes [20,21]. But these methods usually require a specific loading mode and the fabrication process of these structures is quite complicated. Therefore, there is a lot of work devoted to other strategies with controllable adhesion. Recent studies have found that changes in adhesion are related to the strain energy release rate and the stress distribution at the interface [22]. Minsky et al. prepared composite posts consisting of a stiff core and a compliant shell and found that the adhesion was enhanced by adding a stiff core [23]. Bahjepalli and Sarah et al. studied the adhesion enhancement of composite pillars with a different soft tip layer and stiffer stalk interface [24,25]. So tunable adhesion is achieved by the composite structure, such as pressurized structures [26,27], applying thermal fields [28,29]/magnetic field [30,31], and using phase change materials [32–34]. These works provide other ways to control adhesion and each has its own advantages and disadvantages.

Magnetically actuated approaches have the characteristics of fast response and non-contact, thus have great advantages in controlled adhesion. In the previous work, the surface structures/properties were

* Corresponding author. Tel.: +86 551 63600419.
** Corresponding author. Tel.: +86 551 63601236.
E-mail addresses: wyu@ustc.edu.cn (Y. Wang), gongxl@ustc.edu.cn (X. Gong).

https://doi.org/10.1016/j.compscitech.2020.108115
Received 29 December 2019; Received in revised form 7 March 2020; Accepted 10 March 2020
Available online 13 March 2020

switched between adhesive and non-adhesive states by a magnetic field [35,36]. In addition, to drive an object to deform, the magnetic field can directly improve the mechanical properties such as the modulus of the material [37–39]. In this case, a new strategy of controllable adhesion by a magnetic field is proposed in this paper. The magnetically tunable adhesion is achieved by a composite structure that consists of a shell and a magnetic sensitive core. Magnetic sensitive material is used in the preparation of the adhesive structure, the interfacial stress distribution of the structure can be changed by adjusting the magnetic field, thereby changing the adhesion. Magnetorheological polymer gel (MRPG) is a magnetically sensitive gel, which is usually composed of adding micro/nano-sized ferromagnetic particles into a nonmagnetic polymer gel [40,41]. The mechanical properties of MRPG can be adjusted quickly and reversibly by magnetic fields, and the relative magnetorheological effect can reach to 500% [42]. Thus using MRPG as the core of the composite structure can change the interface stress distribution by the magnetic field to adjust the adhesion.

In this paper, a composite pad consisting of a PDMS shell and a soft MRPG core was prepared. The adhesion of the composite pad under different pull off velocities and magnetic field was tested. The stress distribution of composite structures with a soft substrate is different from that of structures with a hard substrate, but there are few studies. In order to study the mechanism of magnetically controllable adhesion, the interfacial stress distribution and out-of-plane displacement of pads under different magnetic fields were calculated by the finite element method. In addition, the shape of the core can also affect the interface stress distribution, thus composite pads with another three core shapes are prepared to optimize the structure design. The adhesion on the uneven surface was also tested. At last, a demonstration of magnetically controlled grabbing and release was done with the pad-bump array.

2. Experiment

2.1. Preparation of MRPG

MRPG was prepared by dispersing carbonyl iron particles (CIP, type CN, provided by BASF in Germany with an average radius of 6 μm) into a homemade polyurethane (PU) gel. The polymer gel was synthesized by a chemical method [43]. The materials used for the synthesis were toluene diisocyanate (TDI, 2,4-TDI at B80%, 2,6-TDI at B20%, Tokyo Chemical Industry Co., Ltd., Japan), polypropylene glycol (PPG-1000, Mr = 1000, Sinopec Group Co., Ltd., China), and 1,4-butanediol (BDO, Mr = 90, Sinopharm Chemical Reagent Co., Ltd., China). Once the PU was synthesized, the CIPs were added to the gel by vigorously stirring until the gel and CIPs were well mixed. MRPGs with CIP volume fraction of 15% and 30% were prepared for use.

2.2. Preparation of composite pads

The composite pads were fabricated following the steps in Fig. 1a. The molds were printed with a 3D printer. PDMS was mixed and stirred with a 10:1 ratio of prepolymer to curing agent for use. Firstly, mold 1 was attached to a glass plate and PDMS was poured into it. The mold 1 has a 3 × 3 cylindrical space. Then, mold 2 was covered on mold 1 and excess PDMS was squeezed out of the gap. The mold 2 has a 3 × 3 protruding cylinder. Each cylinder on mold 2 corresponded to a cylindrical hollow in mold 1. PDMS filled in the gap was cured at 60 °C for 1 h to form a cylindrical shell. After that, mold 2 was removed. MRPG was then dropped into the cavities formed by mold 2. In this step, the MRPG was heated to 60 °C. At this temperature, MRPG is softened and viscous. Then vacuum treatment can make MRPG and PDMS fit closely. The filling height of MRPG can be controlled by controlling the amount of MRPG and the height was 1.2 mm according to the results of finite element analysis (Fig. S1). Then, PDMS was dropped on the MRPG surface and covered the PDMS surface with a piece of glass. At last, the composite was kept at 60 °C for 1 h and removing the glasses gave the final composite pads array. The glass is used up and down to make the surface of the composite structure flat and smooth. The prepared composites pads array has 3 × 3 columnar pads with PDMS shells and MRPG cores. The size parameters of a single pad are shown in Fig. 1b. The thickness of the PDMS layer and MRPG core are t = 0.4 mm and h = 1.2 mm respectively. The diameter of the pad and MRPG core are D = 4.0 mm and d = 3.2 mm. The height of the pad H is 2.4 mm and the edge thickness is 1 mm. The interface between the core and the PDMS is flat, hence the composite pad is called pad flat. What's more, composite pads with different core shapes can be fabricated by changing the protruding structures on the mold 2. Fig. 1c shows a schematic view of composite pads with different core shapes. The structural shapes on the mold 2 are concave, bumpy, and convex, and the corresponding composite pads are called pad-concave, pad-bump, and pad-convex respectively. To better

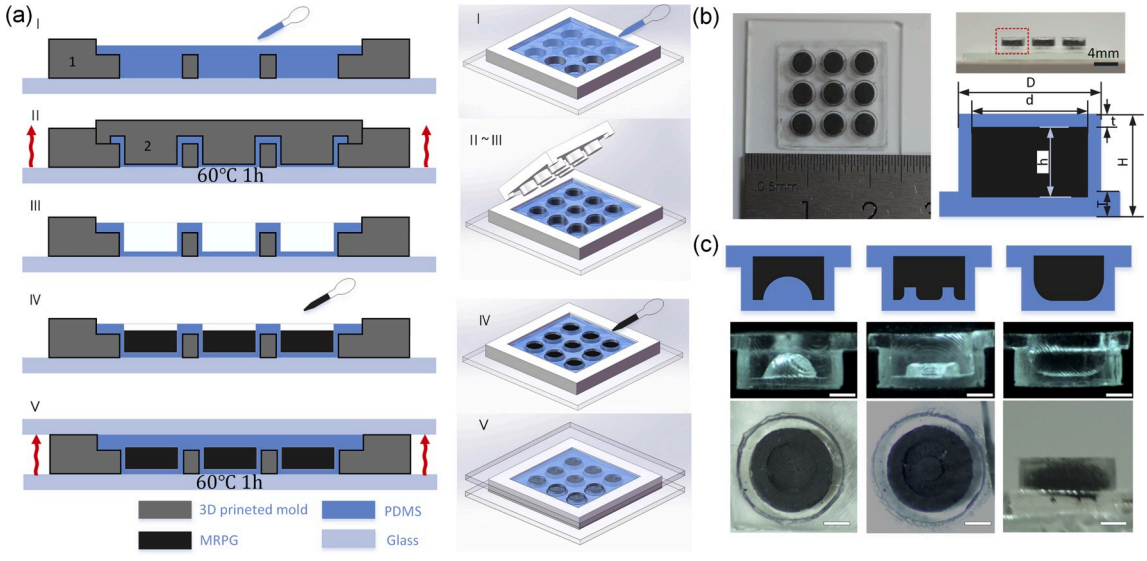

Fig. 1. (a) The preparation process of the composite pads array. (b) A photo of the composite pads array and a schematic of the pad, blue is PDMS and black is MRPG. (c) Schematics of composite pads with different core shapes, the side views of the prepared PDMS shells, the top views of the pad-concave and pad-bump, side view of pad-convex. The scale bar in the figure is 1 mm. (For interpretation of the references to colour in this figure legend, the reader is referred to the Web version of this article.)

observe the internal structure of the composite pads, side views of the PDMS shells and top views of the composite pads are shown in Fig. 1c. As the shape of the mold changes, the structure of the PDMS film on the top of the composite pads changes, which will affect the interface stress distribution. Detailed structures are shown in Fig. S2c.

2.3. Characterization

The adhesion properties of the composite pad were tested by a commercial rheometer (Physica MCR302, Anton Paar GmbH, Austria) equipped with an electro-magnetic accessory (MRD180). The MRD180 module is able to generate different magnetic fields at the platform by setting the current during the test. A single composite pad was cut from the prepared composite pad array for the adhesion test. The composite pad and a glass slide were treated by a plasma cleaner (PDC-36G, MTI Corp.) for 10 s. The composite pad was then placed on the glass and the bottom of the pad was immediately bonded to the glass (Fig. S2a). Bonding the composite pad to the glass sheet is for ease of fixation. During the test, the glass at the bottom of the composite pad was fixed to the platform. A PP20 parallel-plate rotor was employed and the rotor surface was parallel to the bottom plate. A glass was attached to the rotor and the glass surface was also parallel to the surface of the composite pad. The applied current and speed of the rotor could be controlled during the test, the normal force and displacement of the rotor were recorded by the computer. The accuracy of the normal force and displacement is 2 mN and 1 μm respectively. The contact images between the composite pad and the glass were recorded by using the Rheo-Microscope module (Fig. S3). The Rheo-Microscope consists of a CCD camera and a microscope tube (0.7 ×) beneath the glass platform. The illumination lights the sample from below.

The mechanical properties of MRPGs under compression were tested on an electromechanical universal testing machine (Model 43, MTS System Corporation, China, Fig. S4). The MRPG samples were placed between two Helmholtz coils and the initial diameter of the sample was 20 mm and the initial height was 3 mm.

3. Results and discussion

3.1. Adhesion characterization

The adhesion strength of the composite pad was tested on a commercial rheometer with an electro-magnetic accessory MRD180. The composite pad was fixed on the plate of rheometer. The flat glass was attached to the rotor. The rotor was controlled to move up and down and the normal force on the pad was collected. The magnetic field at the sample can be regulated by adjusting the current in the MRD180 module. The magnetic field distribution at the pad was calculated by finite element analysis, and the results showed that 5 A corresponded to about 200 mT, which was the same as the test result. Fig. 2b shows the normal force as the function of time during the loading and detaching process. The whole process can be divided into three procedures. Firstly, the rotor was moved down at a speed of 10 μm/s until the normal force reached about 0.2 N. This process is called the approaching process. The compression displacement at this stage is between 50 μm and 60 μm. Then the position was kept for 30 s to ensure that the pad was in full contact with the glass. The pre-force decreased and gradually tended to stable because of the viscoelastic characteristics of the MRPG inside the pad. The stable force is called the pre-force. In the third stage, the rotor rose at a speed of 40 μm/s and the composite pad was separated from the glass. The maximum tensile force during the separation process is counted as the pull-off force under this speed. In the third stage, controlling the current in the MRD180 module can change the magnetic field and adjust the adhesion.

Due to the viscoelastic nature of MRPG inside the pad, the pre-force for different pads were different at the same displacement. So the influence of pre-force on the adhesion was tested. In Fig. 2c, when the pre-force was increased from 0.064 N to 0.228 N, the pull-off force during the separation process was basically the same, indicating that the

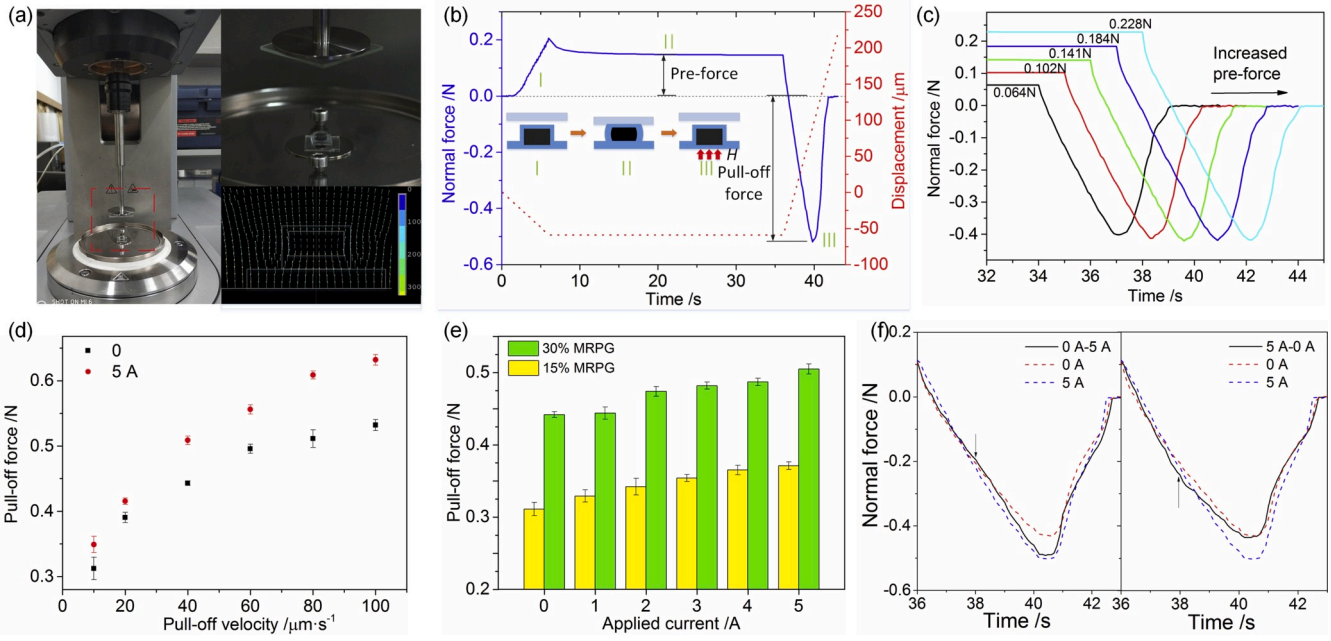

Fig. 2. Adhesion test of pad-flat. (a) Test system and the magnetic field distribution at the sample. (b) The normal force on the pads during the test. The green numbers in the figure are correlated with the experimental procedure 1. Approaching, 2. Preloading, 3. Pull off. During the pull off process, the magnetic field was changed to control the adhesion. The maximum normal force during stretching was called the pull-off force. (c) Pull-off forces of pad-flat with different pre-force. (d) Pull-off forces of pad-flat with 30% MRPG under different pull-off velocities and different applied currents. (e) Pull-off forces of the pad-flats filled with different materials. The pull-off velocity was 40 μm/s 15%MRPG and 30%MRPG means the volume fraction of the carbon iron powders in MRPG is 15% and 30% respectively. (f) The normal force on pad-flat under different applied currents. The solid line shows the result of normal force with changing current during the pull off process. (For interpretation of the references to colour in this figure legend, the reader is referred to the Web version of this article.)

adhesion is not sensitive to the pre-force of this interval. Therefore, the pre-force was maintained at about 0.15 N in the subsequent tests. The adhesion of composite was usually rated dependent [44], so the adhesion under different velocities was tested with and without applied current. It can be seen from Fig. 2d that as the pull-off velocity increased, the adhesion increased. In particular, the adhesion of pad-flat was enhanced by a magnetic field at all pull-off velocities. Generally, the adhesion strength is usually related to the interface stress distribution [45]. The yield stress can be enhanced by a magnetic field. (Fig. S3d). Then the interface stress distribution was changed and the pull-off force was enhanced by the magnetic field. Pad-flats with different filling materials were prepared and tested (Fig. 2e). The pull-off force increases with an increasing yield stress of MRPG in the pads. The mechanical properties of the MRPG depend on the volume fraction of iron powder and the magnetic field. Thus the adhesion can be changed by controlling the iron powder content in the MRPG and adjusting the magnetic field.

The effect of varying magnetic fields on adhesion was also tested. In Fig. 2f, red dash lines and blue dash lines respectively represent the normal force with or without a magnetic field. The solid line shows the result of normal force with changing current. '0 A–5A' means the applied current is changed from 0 A to 5 A at the 38 s and vice versa. In the left picture of Fig. 2f, the current is zero before 38 s. The solid line basically coincides with the red dash line. When the applying currents are changed, the mechanical properties of MRPG will be changed. The change of mechanical properties of MRPG will lead to the change of normal force. It can be found that the solid line basically coincides with the blue dash line after 40 s, which means that the normal force can be controlled to rapidly switch between the two modes. It can be seen from Fig. 2f that it takes about 2 s for the adhesion of the pad to change when the magnetic field changes.

3.2. Interface stress distribution

The change of pull-off force by the magnetic field is due to the change of the stress distribution at the interface, so the normal stress distribution at the interface is calculated by using ABAQUS 6.13. The element type is CAX4R and the mesh size is 0.01 mm. Fig. 3a shows a schematic diagram of finite element modeling. A 2D axisymmetric model is used and the Z-axis represents the axis of symmetry. The Young's modulus of PDMS and glass are 2 MPa and 5.5 GPa, the Poisson's ratio of PDMS and glass are 0.49 and 0.25, respectively. MRPG is regarded as an ideal plastic material with Poisson's ratio of 0.49, Young's modulus of 2, 7, 20, and 20 MPa, and yield stress of 4 kPa, 14 kPa, 21 kPa, and 40 kPa for MRPG-15%-0 A, MRPG-15%-5 A, MRPG-30%-0 A, and MRPG-30%-5 A, respectively. The interface between the PDMS and the MRPG core was assumed to be perfectly bonded. Fig. 3b shows the normalized normal stress distribution at the contact interface with different cores. The stresses are normalized by dividing the local stress σ_z by the average stress σ_{zc} at the interface. The normalized stresses increase with R and reach the maximum at the edge for all the samples with soft cores. Therefore, in the process of separation, cracks first appear at the edge. Compared with Fig. 3c, it can be found that with the increasing yield stress of MRPG core, the normalized stress at the edge decreases and the pull-off force increases. The smaller the edge stress is, the more uniform the stress distribution is, so it can bear more tension. At the same time, when the yield stress increases, the equivalent modulus of the pad

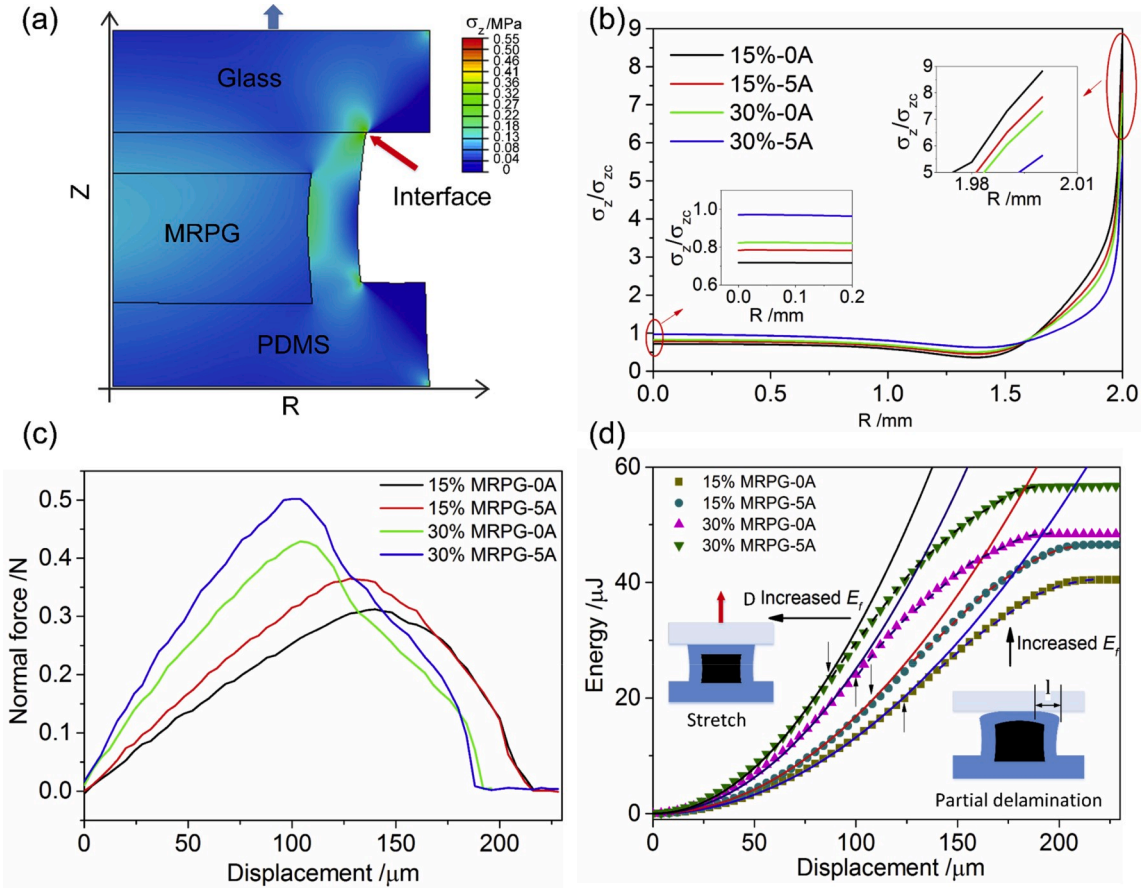

Fig. 3. (a) Schematic diagram of finite element modeling. A 2D axisymmetric model was used and the Z-axis represents the axis of symmetry. (b) The finite element analysis results of the normalized normal stress σ_z/σ_{zc} distribution at the contact interface of the composite pads with different cores. (c) Normal forces on the pad-flats with different cores. Here, the normal force when the sample was pulled off was recorded as a positive value. (d) Energy during the pulled off process. The arrow indicates the position of the inflection point, and the slope of the inflection point corresponds to the pull-off force.

increases, so the slope of the normal force curve increases. It can also be seen from the energy change in Fig. 3d that the whole separation process can be divided into two steps. First, as the displacement increases, the pad is stretched but the pad surface remains in full contact with the glass surface. In this process, the sample is stretched and the energy curve is a parabola. As the displacement increases, the stress at the edge reaches critical value and cracks will initiate, which causes delamination. The change of curve trend in Fig. 3d reflects the change of energy form in two stages. The arrow in Fig. 3d indicates the position of the inflection point, and the slope of the inflection point corresponds to the pull-off force. The specific form of energy cannot be obtained because the deformation of PDMS and MRPG during the delamination process is difficult to calculate. However, as the modulus of the filler MRPG increases, the energy required for the same deformation increases. Therefore, the slope at the inflection point increases and the corresponding displacement decreases, which is consistent with the previous analysis results.

3.3. Effect of magnetic field loading mode

Applying a magnetic field during the pull off process can increase the modulus of the core and increase the adhesion of the composite pad. At the same time, it is also found that changing the loading mode of the magnetic field can also adjust the adhesion of the composite pad. Fig. 4a shows another loading mode of the magnetic field. The current is applied during the first two processes. This magnetic field loading mode is called 'pre-5 A'. Fig. 4b shows the pull-off force is less than that with a 5 A magnetic field. The two magnetic fields have the same intensity, but the timing of the application is different, resulting in different adhesion. We find that under a 'pre-5 A' magnetic field, a depression occurs at the center of the flat surface. Under the action of the magnetic field, the MRPG core is attracted by the magnetic field, which causes the PDMS shell to deform. So the attracted force is firstly calculated, and then the deformation under this force is simulated. The attracted force is 0.025 N as a body force. Fig. 4d shows the out-of-plane displacement. After the action of a 'pre-5 A' magnetic field, the center of the pad surface is lower than the edge of the pad surface before contacting, which will increase the stress at the edge after contacting. For composite pads with soft cores, the normal stress at the edge is the maximum, so the increased stress at the edge will increase the nonuniformity of stress distribution, which in turn decreases the adhesion.

3.4. Effect of core shapes

The adhesion of the composite pad is dependent on the interface stress distribution, and the core shape of the pad also has an effect on the interface stress distribution, which in turn affected adhesion. Therefore, composite pads with another three core shapes were prepared to optimize the structure design. In order to reduce the inhomogeneity of the magnetic field and ensure the same wall thickness of PDMS, three axisymmetric core shapes are selected. The adhesion strength of composite pads with different core shapes was tested under different magnetic fields and the pull-off forces were shown in Fig. 5b. Here, '5 A' means the magnetic field is generated by applying a 5 A current in the coil during the pull off process. The detailed normal force is shown in Fig. S5. The results show that the pull-off force of pad-concave is the largest with or without a magnetic field. According to the results of the finite element analysis in Fig. 5a, it can be seen that the ratio of interface boundary stress σ_{ze} to average stress σ_{zc} of pad-concave is the smallest with or without a magnetic field, so its adhesion is the largest. Here the interface normal stress reaches the maximum at the boundary ($R = 2$

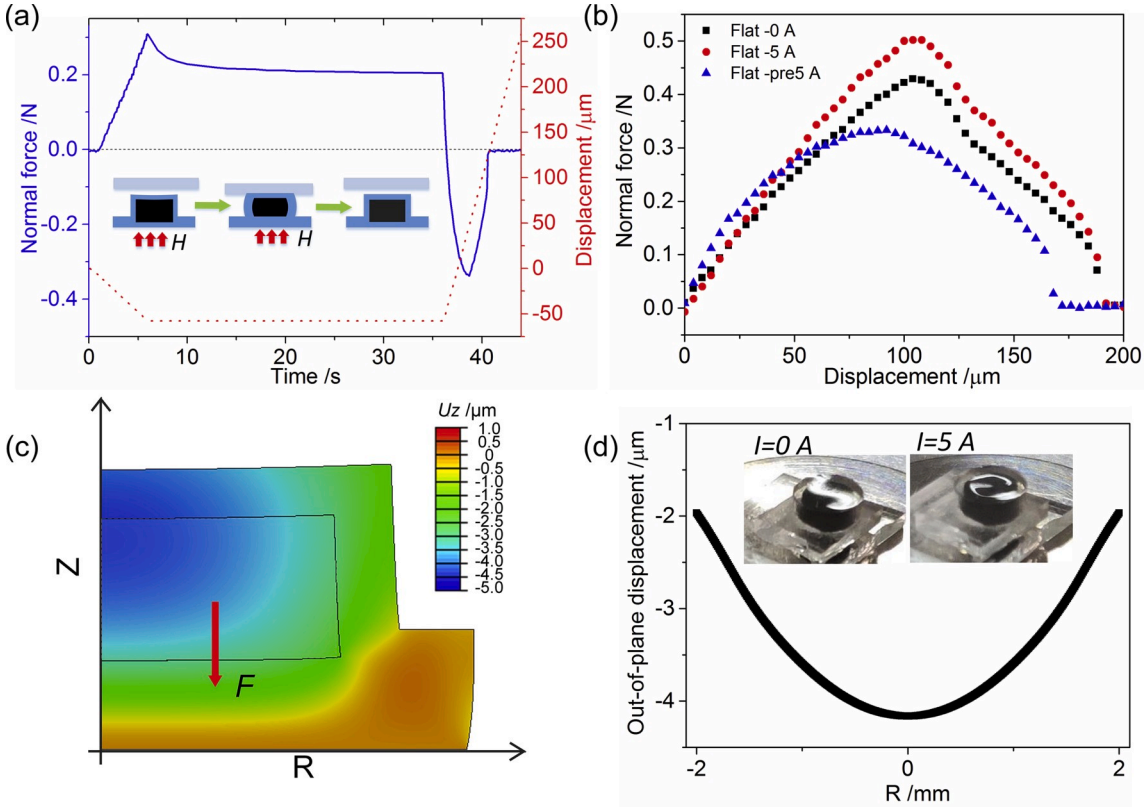

Fig. 4. (a) Another magnetic loading mode. During the test, the current was applied during the first two processes. The maximum normal force under this magnetic field loading mode is called the pull-off force of pre-5 A. (b) The normal force on pad-flat under different magnetic field loading modes. (c) Schematic diagram of finite element modeling of surface deformation. The MRPG is attracted by a downward force. The force was firstly calculated, and then the deformation under this force was simulated. (d) The finite element modeling results of out-of-plane displacement under a pre-5 A magnetic field. Illustration in the picture shows the surface is no longer flat under the action of a magnetic field.

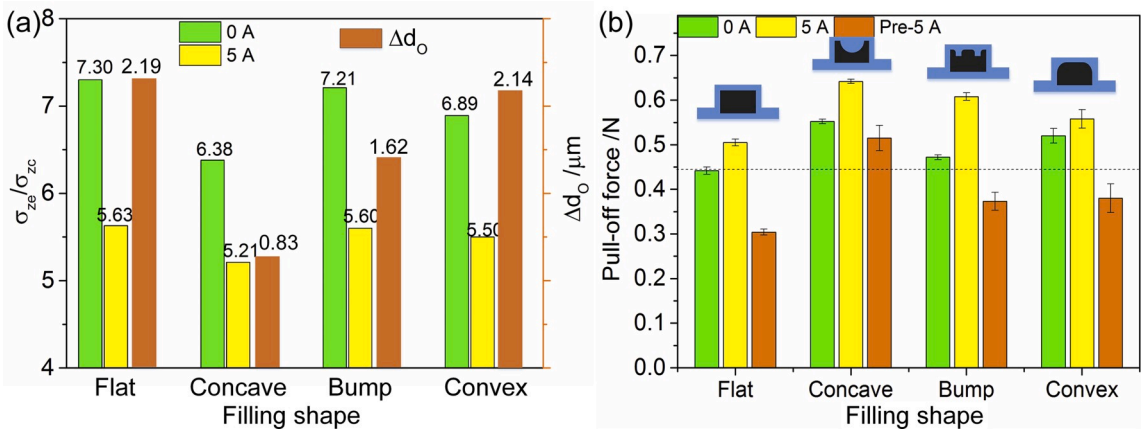

Fig. 5. (a) Results of finite element analysis of composite pads with different core shapes: Yellow square and green square represent the ratios of interface boundary stress σ_{ze} to average stress σ_{zc} with or without a magnetic field. The orange square represents the height difference Δd_o between the edge ($R = 2$ mm) and the center ($R = 0$ mm) of the composite pad under a 'pre-5 A' magnetic field. (b) Pull-off forces for composite pads with different core shapes under different magnetic fields. (For interpretation of the references to colour in this figure legend, the reader is referred to the Web version of this article.)

mm), so the ratio of the interface stress to the average stress at the boundary is calculated. At the same time, the height difference Δd_o of pad-concave under a 'pre-5 A' magnetic field is the smallest, so the decrease of pull-off force is the smallest. The detailed deformation results are shown in Fig. S6. Similarly, because the ratio σ_{ze}/σ_{zc} and height difference Δd_o of pad-flat are the largest, its pull-off force is the smallest under different magnetic fields. In summary, the pull-off force increases with the decreasing ratio of σ_{ze}/σ_{zc} and height difference Δd_o. So the adhesion of the composite pad can be enhanced or reduced by adjusting the magnetic field and the adjustment range of the pull-off force by the magnetic field is related to the core shape of the composite pad. In particular, for pad-bump, the pull-off force can be controlled to change between 0.373 N and 0.608 N by adjusting the magnetic field, with the largest range of magnetic field adjustment.

3.5. Adhesion on uneven surface

In addition to the magnetically tunable adhesion, the use of MRPG as

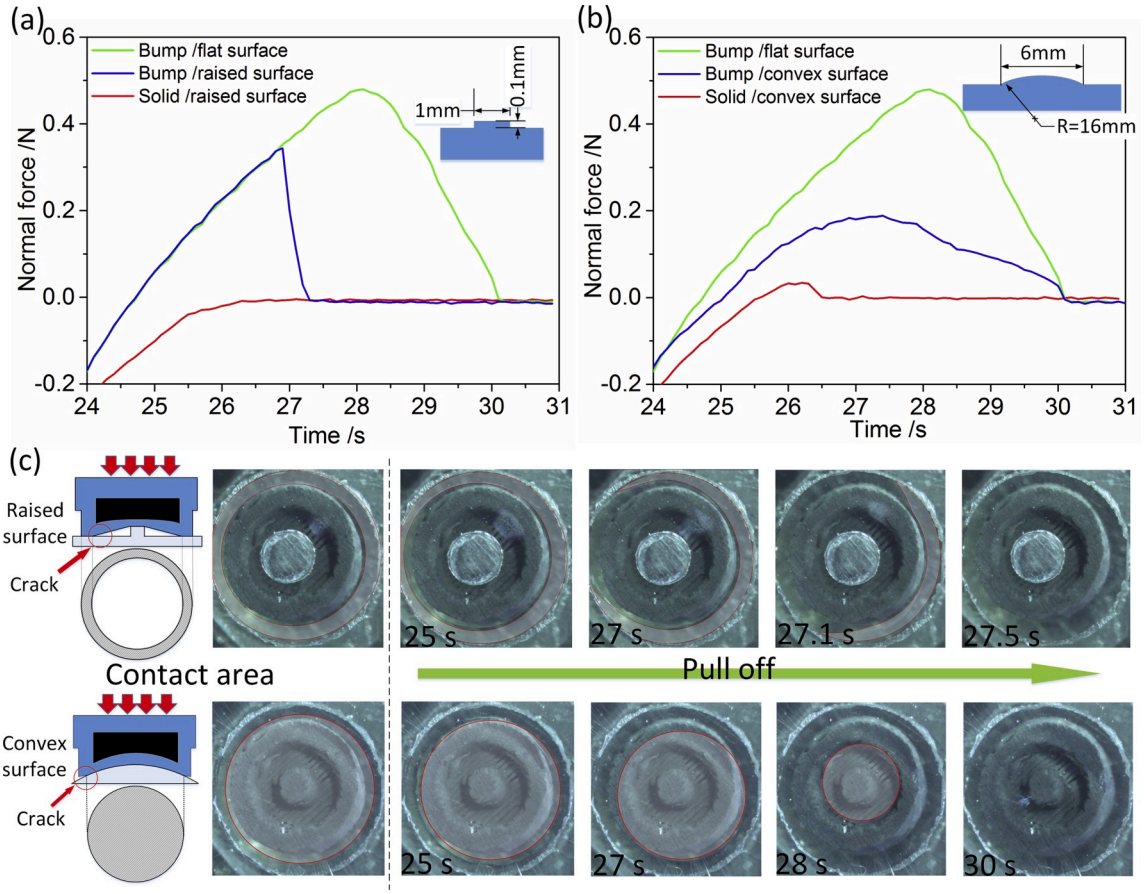

Fig. 6. Adhesion test between pad-bump and uneven surface: (a) raised surface, (b) convex surface. (c) Images of the contact between pad-bump and uneven surface during the test.

a soft core can also improve the adhesion of the pad to uneven surfaces [46]. Two kinds of uneven surfaces were used in the experiments. A thin film with a diameter of 1 mm and a thickness of 0.1 mm was put on the glass surface to make a raised surface and the convex surface was made of a polymethyl methacrylate (PMMA) plate. During the test, pad-bump was controlled to contact the uneven surface at the speed of 10 μm/s. When the force reached 0.2 N, space was kept for 20 s, and then the sample was lifted at the speed of 40 μm/s. The experimental setup is shown in Fig. S2. As shown in Fig. 6a, the adhesion of the solid core pad is substantially zero but the pad-bump still has a certain adhesion to the raised surface. The solid core pad is the pad manufactured by PDMS only. During the approaching process, the surface of the solid core pad is difficult to deform, and there is almost no contact with the glass surface. But for pad-bump with a soft core, the center portion of the pad is recessed during contact, and the edge region of the pad can be in contact with the surface of the glass. As shown in Fig. 6c, due to the presence of the thin film, there is a gap between the center of the pad and the surface of the glass after the preloading process. During the pull off process, the crack first expands from the center rather than the edge of the pad, which will cause the normal force to decrease in advance. So compared to the flat plane, the normal force curves in Fig. 6a are coincident until the normal force reached a maximum. Images of contact on flat and raised surfaces are shown in Videos S1 and S2 separately.

Supplementary video related to this article can be found at https://doi.org/10.1016/j.compscitech.2020.108115.

Similarly, on convex surfaces, the composite pad has greater adhesion than a solid core pad. For the convex surface, the contact area is larger than that of the solid core pad because the core of the pad is softer. But it is not completely in contact, there is a gap at the edge of the interface after preloading. Thus cracks are easier to expand from the edges during stretching. It is also worth noting that the crack expands at the beginning of the pulled off process (Video S3), which makes the slope of the normal force curve in Fig. 6b smaller than that on a flat surface. In addition, the contact area on the convex surface is larger than that on the raised surface but the adhesion of the composite pad is smaller than the adhesion on a raised surface. It indicates that the composite pad has a strong anti-interference ability to the central area and is sensitive to stress concentration at the edge.

Supplementary video related to this article can be found at https://doi.org/10.1016/j.compscitech.2020.108115

3.6. Demonstration of magnetically controlled grabbing and release

To demonstrate the application of the composite pad array for use in pick-and-place area, an experimental setup for magnetic field controlled grabbing and release was shown in Fig. S7. The normal forces on pad-bump array under different applied currents was firstly tested. The result in Fig. S7a shows the pull-off force increases from 3.14 N to 5.36 N by adjusting the current. In the demonstration experiment, a pad-bump array was attached to an electromagnet. The power supply was used to apply current in the electromagnet. The quartz sheet was adhered to the surface of the aluminum plate as a weight to be grasped. Video S4 shows that under a magnetic field of pre-5 A, the adhesion of the pad array is not sufficient to grasp the weight. But when applying a 5 A magnetic field, the array can pick up a 173 g mass and hold it. If you want to release the object, cut off the current, the weight will fall off within 2 s (Video S5). There is a difference between the weight that the array can grab and the pull-off force of a single pad because it is difficult to ensure that the array is parallel to the object during actual operation. However, the control result of the magnetic field is still obvious, and the response speed is fast under the control of the magnetic field.

Supplementary video related to this article can be found at https://doi.org/10.1016/j.compscitech.2020.108115

4. Conclusion

In this paper, a novel structure array with a 3 × 3 composite pad is prepared to achieve adhesion tunability. Each pad in the array consists of a PDMS shell and a soft MRPG core. The use of soft MRPG as the core makes the adhesion of the composite pad sensitive to the magnetic field. On one hand, the pull-off force of the composite pad can be improved under applying a magnetic field. The pull-off force increases from 0.442 ± 0.008 N to 0.505 ± 0.007 N by applying a current of 5 A. The modulus and yield stress of the MRPG inside the pad are increased by the magnetic field and the normalized normal stress at the edge decreases, so the pull-off force increases. On another hand, the adhesion of the composite pad can be reduced under another magnetic field loading mode. The surface of the pad deforms under the action of a magnetic field, thus the edge stress of the pad is increased by applying a magnetic field after contacting, which causes a decrease in adhesion. The larger the initial deformation, the smaller the adhesion. In addition, the effect of core shapes on the adhesion of composite pad is studied. The range of magnetically tunable adhesion for pad-bump was the largest. The application of the soft core also improved the adhesion of the composite pad to uneven surfaces compared to that of structures with hard core [47]. In summary, the adhesion of the composite pad can be enhanced or reduced by adjusting the magnetic field. In particular, for a pad-bump array, the adhesion can be controlled to change between 3.14 N and 5.36 N by adjusting the magnetic field, which makes it great potential in pick-and-place applications.

Declaration of competing interest

The authors declare that they have no known competing financial interests or personal relationships that could have appeared to influence the work reported in this paper.

CRediT authorship contribution statement

Haoming Pang: Conceptualization, Investigation, Methodology, Software, Writing - original draft. **Lei Pei:** Formal analysis, Data curation. **Jiaqi Xu:** Visualization, Investigation. **Saisai Cao:** Software, Formal analysis. **Yu Wang:** Project administration, Software, Validation, Writing - review & editing. **Xinglong Gong:** Supervision, Resources, Writing - review & editing.

Acknowledgements

This work was supported by the National Natural Science Foundation of China (Grant Nos. 11572310, 11822209), the Fundamental Research Funds for the Central Universities (WK2090000015) and the Strategic Priority Research Program of the Chinese Academy of Sciences (Grant No. XDB22040502). This study was also supported by the Collaborative Innovation Center of Suzhou Nano Science and Technology.

Appendix ASupplementary data

Supplementary data to this article can be found online at https://doi.org/10.1016/j.compscitech.2020.108115.

References

[1] C.H. Lee, D.R. Kim, X.L. Zheng, Fabricating nanowire devices on diverse substrates by simple transfer-printing methods, Proc. Natl. Acad. Sci. U.S.A. 107 (22) (2010) 9950–9955.
[2] C.H. Linghu, S. Zhang, C.J. Wang, J.Z. Song, Transfer printing techniques for flexible and stretchable inorganic electronics, npj Flex. Electron. 2 (2018) 26.
[3] Y.A. Huang, H. Wu, L. Xiao, Y.Q. Duan, H. Zhu, J. Bian, D. Ye, Z.P. Yin, Assembly and applications of 3D conformal electronics on curvilinear surfaces, Mater. Horizons 6 (4) (2019) 642–683.
[4] H.Y. Luo, C.J. Wang, C.H. Linghu, K.X. Yu, C. Wang, J.Z. Song, Laser-driven programmable non-contact transfer printing of objects onto arbitrary receivers via

an active elastomeric micro-structured stamp, National Science Review (2019), https://doi.org/10.1093/nsr/nwz109.
[5] Y. Zhang, B.W. Lu, T. Wang, X. Feng, H.X. Xu, A Photochemical approach toward high-fidelity programmable transfer printing, Adv. Mater. Technol. 4 (9) (2019), 1900163.
[6] Y.C. Chen, H.T. Yang, Octopus-inspired assembly of nanosucker arrays for dry/wet adhesion, ACS Nano 11 (6) (2017) 5332–5338.
[7] H.E. Jeong, J.K. Lee, H.N. Kim, S.H. Moon, K.Y. Suh, A nontransferring dry adhesive with hierarchical polymer nanohairs, Proc. Natl. Acad. Sci. U.S.A. 106 (14) (2009) 5639–5644.
[8] M.P. Murphy, C. Kute, Y. Menguc, M. Sitti, Waalbot II: adhesion recovery and improved performance of a climbing robot using fibrillar adhesives, Int. J. Robot Res. 30 (1) (2011) 118–133.
[9] A.M. Nasab, A. Sabzehzar, M. Tatari, C. Majidi, W.L. Shan, A soft gripper with rigidity tunable elastomer strips as ligaments, Soft Robot. 4 (4) (2017) 411–420.
[10] J.M.R. Bullock, W. Federle, Beetle adhesive hairs differ in stiffness and stickiness: in vivo adhesion measurements on individual setae, Naturwissenschaften 98 (5) (2011) 381–387.
[11] H.B. Zeng, N. Pesika, Y. Tian, B.X. Zhao, Y.F. Chen, M. Tirrell, K.L. Turner, J. N. Israelachvili, Frictional adhesion of patterned surfaces and implications for gecko and biomimetic systems, Langmuir 25 (13) (2009) 7486–7495.
[12] R. Hensel, K. Moh, E. Arzt, Engineering micropatterned dry adhesives: from contact theory to handling applications, Adv. Funct. Mater. 28 (28) (2018), 1800865.
[13] L.F. Boesel, C. Greiner, E. Arzt, A. del Campo, Gecko-inspired surfaces: a path to strong and reversible dry adhesives, Adv. Mater. 22 (19) (2010) 2125–2137.
[14] M.P. Murphy, B. Aksak, M. Sitti, Gecko-inspired directional and controllable adhesion, Small 5 (2) (2009) 170–175.
[15] C. Pang, M.K. Kwak, C. Lee, H.E. Jeong, W.G. Bae, K.Y. Suh, Nano meets beetles from wing to tiptoe: versatile tools for smart and reversible adhesions, Nano Today 7 (6) (2012) 496–513.
[16] Y. Cho, H.K. Minsky, Y.J. Jiang, K.Y. Yin, K.T. Turner, S. Yang, Shear adhesion of tapered nanopillar arrays, ACS Appl. Mater. Interfaces 10 (13) (2018) 11391–11397.
[17] Z.Z. Wang, Slanted functional gradient micropillars for optimal bioinspired dry adhesion, ACS Nano 12 (2) (2018) 1273–1284.
[18] J. Purtov, M. Frensemeier, E. Kroner, Switchable adhesion in vacuum using bio-inspired dry adhesives, ACS Appl. Mater. Interfaces 7 (43) (2015) 24127–24135.
[19] C.T. Bauer, E. Kroner, N.A. Fleck, E. Arzt, Hierarchical macroscopic fibrillar adhesives: in situ study of buckling and adhesion mechanisms on wavy substrates, Bioinspiration Biomimetics 10 (6) (2015), 066002.
[20] A. Carlson, H.J. Kim-Lee, J. Wu, P. Elvikis, H.Y. Cheng, A. Kovalsky, S. Elgan, Q. M. Yu, P.M. Ferreira, Y.G. Huang, K.T. Turner, J.A. Rogers, Shear-enhanced adhesiveless transfer printing for use in deterministic materials assembly, Appl. Phys. Lett. 98 (26) (2011), 264104.
[21] S.Y. Yang, A. Carlson, H.Y. Cheng, Q.M. Yu, N. Ahmed, J. Wu, S. Kim, M. Sitti, P. M. Ferreira, Y.G. Huang, J.A. Rogers, Elastomer surfaces with directionally dependent adhesion strength and their use in transfer printing with continuous roll-to-roll applications, Adv. Mater. 24 (16) (2012) 2117–2122.
[22] N.A. Fleck, S.N. Khaderi, R.M. McMeeking, E. Arzt, Cohesive detachment of an elastic pillar from a dissimilar substrate, J. Mech. Phys. Solid. 101 (2017) 30–43.
[23] H.K. Minsky, K.T. Turner, Achieving enhanced and tunable adhesion via composite posts, Appl. Phys. Lett. 106 (20) (2015), 201604.
[24] S.C.L. Fischer, E. Arzt, R. Hensel, Composite pillars with a tunable interface for adhesion to rough substrates, ACS Appl. Mater. Interfaces 9 (1) (2017) 1036–1044.
[25] R.G. Bahjepalli, S.C.L. Fischer, R. Hensel, R.M. McMeeking, E. Arzt, Numerical study of adhesion enhancement by composite fibrils with soft tip layers, J. Mech. Phys. Solid. 99 (2017) 357–378.
[26] A. Carlson, S.D. Wang, P. Elvikis, P.M. Ferreira, Y.G. Huang, J.A. Rogers, Active, Programmable elastomeric surfaces with tunable adhesion for deterministic assembly by transfer printing, Adv. Funct. Mater. 22 (21) (2012) 4476–4484.
[27] S. Song, D.M. Drotlef, C. Majidi, M. Sitti, Controllable load sharing for soft adhesive interfaces on three-dimensional surfaces, Proc. Natl. Acad. Sci. U.S.A. 114 (22) (2017) E4344–E4353.
[28] S. Kim, M. Sitti, T. Xie, X.C. Xia, Reversible dry micro-fibrillar adhesives with thermally controllable adhesion, Soft Matter 5 (19) (2009) 3689–3693.
[29] H. Keum, Z.N. Yang, K.W. Han, D.E. Handler, T.N. Nguyen, J. Schutt-Aine, G. Bahl, S. Kim, Microassembly of heterogeneous materials using transfer printing and thermal processing, Sci. Rep. 6 (2016) 29925.
[30] J. Krahn, E. Bovero, C. Menon, Magnetic field switchable dry adhesives, ACS Appl. Mater. Interfaces 7 (4) (2015) 2214–2222.
[31] A.G. Gillies, J. Kwak, R.S. Fearing, Controllable particle adhesion with a magnetically actuated synthetic gecko adhesive, Adv. Funct. Mater. 23 (26) (2013) 3256–3261.
[32] Z. Ye, G.Z. Lum, S. Song, S. Rich, M. Sitti, Phase change of gallium enables highly reversible and switchable adhesion, Adv. Mater. 28 (25) (2016) 5088–5092.
[33] M. Tatari, A.M. Nasab, K.T. Turner, W.L. Shan, Dynamically tunable dry adhesion via subsurface stiffness modulation, Adv. Mater. Interf. 5 (18) (2018), 1800321.
[34] J. Krahn, D. Sameoto, C. Menon, Controllable biomimetic adhesion using embedded phase change material, Smart Mater. Struct. 20 (1) (2011), 015014.
[35] D.M. Drotlef, P. Blumler, A. del Campo, Magnetically actuated patterns for bioinspired reversible adhesion (Dry and Wet), Adv. Mater. 26 (5) (2014) 775–779.
[36] C.H. Linghu, C.J. Wang, N. Cen, J.M. Wu, Z.F. Lai, J.Z. Song, Rapidly tunable and highly reversible bio-inspired dry adhesion for transfer printing in air and a vacuum, Soft Matter 15 (1) (2019) 30–37.
[37] Y.C. Li, J.C. Li, W.H. Li, H.P. Du, A state-of-the-art review on magnetorheological elastomer devices, Smart Mater. Struct. 23 (12) (2014), 123001.
[38] J.R. Yao, Y.Y. Sun, Y. Wang, Q. Fu, Z.Y. Xiong, Y.Q. Liu, Magnet-induced aligning magnetorheological elastomer based on ultra-soft matrix, Compos. Sci. Technol. 162 (2018) 170–179.
[39] M. Yu, S. Qi, J. Fu, M. Zhu, D. Chen, Understanding the reinforcing behaviors of polyaniline-modified carbonyl iron particles in magnetorheological elastomer based on polyurethane/epoxy resin IPNs matrix, Compos. Sci. Technol. 139 (2017) 36–46.
[40] H.M. Pang, L. Pei, C.L. Sun, X.L. Gong, Normal stress in magnetorheological polymer gel under large amplitude oscillatory shear, J. Rheol. 62 (6) (2018) 1409–1418.
[41] S. Qi, J. Fu, Y.P. Xie, Y.P. Li, R.Y. Gan, M. Yu, Versatile magnetorheological plastomer with 3D printability, switchable mechanics, shape memory, and self-healing capacity, Compos. Sci. Technol. 183 (2019).
[42] Y.G. Xu, X.L. Gong, S.H. Xuan, W. Zhang, Y.C. Fan, A high-performance magnetorheological material: preparation, characterization and magnetic-mechanic coupling properties, Soft Matter 7 (11) (2011) 5246–5254.
[43] J.Q. Xu, P.F. Wang, H.M. Pang, Y.P. Wang, J. Wu, S.H. Xuan, X.L. Gong, The dynamic mechanical properties of magnetorheological plastomers under high strain rate, Compos. Sci. Technol. 159 (2018) 50–58.
[44] A. Sofla, E. Seker, J.P. Landers, M.R. Begley, PDMS-glass interface adhesion energy determined via comprehensive solutions for thin film Bulge/Blister tests, J. Appl. Mech. 77 (3) (2010), 031007.
[45] M.D. Bartlett, A.J. Crosby, Scaling normal adhesion force capacity with a generalized parameter, Langmuir 29 (35) (2013) 11022–11027.
[46] A.B. Croll, N. Hosseini, M.D. Bartlett, Switchable adhesives for multifunctional interfaces, Adv. Mater. Technol. 4 (8) (2019), 1900193.
[47] S.C.L. Fischer, K. Gross, O.T. Abad, M.M. Becker, E. Park, R. Hensel, E. Arzt, Funnel-shaped microstructures for strong reversible adhesion, Adv. Mater. Interf. 4 (20) (2017), 1700292.